Heliyon 10 (2024) e28874

Contents lists available at ScienceDirect

Heliyon

journal homepage: www.cell.com/heliyon

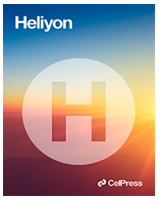

Research article

Differences of individual gray matter networks between MCI patients who converted to AD within 3 Years and nonconverters

Baiwan Zhou, Yueqi Zhao, Xiaojia Wu *

Department of Radiology, the Second Affiliated Hospital of Chongqing Medical University, Chongqing, China

ARTICLE INFO

Keywords:
Mild cognitive impairment
Conversion
Neuroimaging
Connectome
Structural magnetic resonance imaging
Gradient
Topology
Support vector machine

ABSTRACT

Objective: Here we aimed to explore the differences in individual gray matter (GM) networks at baseline in mild cognitive impairment patients who converted to Alzheimer's disease (AD) within 3 years (MCI-C) and nonconverters (MCI-NC).

Materials and methods: Data from 461 MCI patients (180 MCI-C and 281 MCI-NC) were obtained from the Alzheimer's Disease Neuroimaging Initiative (ADNI). For each subject, a GM network was constructed using 3D-T1 imaging and the Kullback–Leibler divergence method. Gradient and topological analyses of individual GM networks were performed, and partial correlations were calculated to evaluate relationships among network properties, cognitive function, and apolipoprotein E (APOE) ϵ4 alleles. Subsequently, a support vector machine (SVM) model was constructed to discriminate the MCI-C and MCI-NC patients at baseline.

Results: The gradient analysis revealed that the principal gradient score distribution was more compressed in the MCI-C group than in the MCI-NC group, with scores for the left lingual gyrus, right fusiform gyrus and left middle temporal gyrus being increased in the MCI-C group ($p < 0.05$, FDR corrected). The topological analysis showed significant differences in nodal efficiency in four nodes between the two groups. Furthermore, the regional gradient scores or nodal efficiency were found to be significantly related to the neuropsychological test scores, and the left middle temporal gyrus gradient scores were positively associated with the number of APOE ϵ4 alleles ($r = 0.192$, $p = 0.002$). Ultimately, the SVM model achieved a balanced accuracy of 79.4% in classifying MCI-C and MCI-NC patients ($p < 0.001$).

Conclusion: The whole-brain GM network hierarchy in the MCI-C group was more compressed than that in the MCI-NC group, suggesting more serious cognitive impairments in the MCI-C group. The left middle temporal gyrus gradient scores were related to both cognitive function and APOE ϵ4 alleles, thus serving as potential biomarkers distinguishing MCI-C from MCI-NC at baseline.

1. Introduction

Alzheimer's disease (AD) is a progressive disease that imposes a heavy economic burden on the health care system [1]. Mild cognitive impairment (MCI) is considered the prodromal stage of AD and is characterized by cognitive changes in memory, language, or another mental function that can be detected by other individuals or clinical tests [2]. Although the global prevalence of MCI is as

* Corresponding author.
E-mail address: 304831@hospital.cqmu.edu.cn (X. Wu).

https://doi.org/10.1016/j.heliyon.2024.e28874
Received 7 November 2023; Received in revised form 24 March 2024; Accepted 26 March 2024
Available online 29 March 2024

high as 6.7–25.2% [3], and that the prevalence increased with age, it is often trivialized because it does not interfere with a person's daily activities. However, in the long term, MCI requires individuals to remain vigilant; during a 3-year follow-up period, approximately 30.9% of MCI patients will progress to AD, which is irreversible and lacks effective treatment options [4]. As such, it is imperative to identify biomarkers that can differentiate MCI patients who will convert to AD (MCI-C) from those who will not convert to AD (MCI-NC) as early as possible and to implement more aggressive preventive treatments to prevent further decline in cognitive functions.

A recent study suggested that the decline of cognitive functions is related to disconnections of the whole brain network [5]. Notably, the connectome approach [6] can noninvasively investigate brain connections by characterizing brain anatomy as a complex network based on different modalities of magnetic resonance imaging (MRI), thus providing a vital tool for exploring biomarkers of cognitive impairment. Compared to functional networks based on resting-state functional MRI or white matter networks based on diffusion tensor imaging, gray matter (GM) networks based on structural MRI are more stable and convenient [7,8], and it has been reported to be related with impaired cognition and pathological biomarkers in the progression of AD [9,10]. Previously, GM networks have usually been constructed by calculating interregional morphological correlations to form a structural covariance network [11]; in this way, a single brain network for a given subject group could be constructed [12], but the individual network of each subject could not be examined and correlated with clinical variables. Therefore, Tijms et al. [13] developed a cube-based method to construct individual morphological networks, but GM networks could not be normalized using this method; therefore, the network measures would be influenced by the size of individual subjects' networks [14]. Thus, the Kullback–Leibler divergence-based similarity (KLS) method has been proposed to perform the normalization of GM networks [15–17] and has been successfully used in the connectome study of neurodegenerative disease [18] and cognitive impairment [19].

Topological properties are the most commonly used measures in the connectome approach; they can be used to investigate the segregation and integration of a complex network [20], alterations of topological properties of GM network in MCI patients have been extensively reported in previous studies [10,21,22], and differences of topological properties of GM network between MCI-C and MCI-NC have also been reported [23], the result suggested topological properties of GM network might have use in identifying MCI-C and MCI-NC patients; however, topological analysis overlooked the hierarchy of brain networks, previous studies have suggested that there is a principal gradient based on the differentiation of connectivity patterns in whole brain networks, ranging from within low-level sensory systems on the one end to the *trans*-modal default mode network (DMN) on the other end [24], gradient analysis may provide insights into how structural distribution of different neural system relate to complex cognitve function [25], and further our understanding of the neural changes associated with cognitive decline. Alterations of the principal gradient have been also reported to be closely related to cognitive decline [26] and mental disorders [27] in previous studies.Therefore, we hypothesize that combining gradient and topological analyses may yield a more comprehensive set of neuroimaging biomarkers for the early differentiation between MCI-C and MCI-NC at the initial stage.

In this study, we aimed to (1) explore the differences in individual GM networks between MCI-C and MCI-NC patients by combining gradient and topological analyses, (2) explore the relationship between the gradient and topological properties and the scores of neuropsychological tests and the number of apolipoprotein E (APOE) €4 alleles, which was the strongest genetic risk factor associated with AD [28], and (3) construct and validate a support vector machine (SVM) model to discriminate the MCI-C group from the MCI-NC group at baseline based on individual GM connectomes.

2. Materials and methods

2.1. Participants

All data used in the current study were obtained from the Alzheimer's Disease Neuroimaging Initiative (ADNI) database (adni.loni.usc.edu). The ADNI study was approved by an ethics standards committee for human experimentation at each institution. Written informed consent was obtained from all participants.

Data from 461 MCI patients, i.e., 180 MCI patients converting to AD during a 3-year follow-up period and 281 MCI patients not converting to AD, were obtained from the ADNI database. The diagnosis of AD was made according to the criteria made by the National Institute of Neurological and Communicative Disorders and Stroke and Alzheimer's Disease and Related Disorders Association.

The demographic and neuropsychological data as well as APOE€4 allele data of all patients were obtained. Eight neuropsychological scales were adopted to evaluate cognitive function; these included the Mini-Mental State Exam (MMSE), Montreal Cognitive Assessment (MoCA), several variants of the Rey Auditory Verbal Learning Test (RAVLT: RAVLT immediate recall, RAVLT learning, RAVLT forgetting, RAVLT percent forgetting), Alzheimer's Disease Assessment Scale Cognitive subscale 11 (ADAS-Cog11) and Alzheimer's Disease Assessment Scale Cognitive subscale 13 (ADAS-Cog13).

2.2. MRI data acquisition

For each participant, three-dimensional T1 weighted imaging (3D-T1) was performed by volumetric three-dimensional magnetization-prepared rapid gradient-echo (3D-MPRAGE) or an equivalent scheme, with slightly different resolutions; this data was obtained from the ADNI database. Three different MR scanners were used in the acquisition of three-dimensional T1-weighted imaging. The MR images acquired using scanner 1 (Siemens Medical Solutions) were scanned with the following parameters: repetition time [TR]/echo time [TE] = 2300.0/3.0 msec and matrix = 240 × 256 × 176. The MR images acquired using scanner 2 (General Electric Healthcare) were scanned with the following parameters: TR/TE = 7.7–7.0/3.1–2.8 msec and matrix = 256 × 256 × 196. The MR images acquired

using scanner 3 (Philips Medical Systems) were scanned with the following parameters: TR/TE = 6.8/3.1 msec and matrix = 256 × 256 × 170.

More detailed information about the image acquisition procedures is available on the ADNI website (http://adni.loni.usc.edu/methods/documents/).

2.3. MRI data preprocessing

The 3D T1-weighted images were preprocessed using the Diffeomorphic Anatomical Registration Through Exponentiated Lie Algebra (DARTEL) toolbox based on Statistical Parametric Mapping (SPM) version 12. Please see the supplemental materials for details.

2.4. Construction of the GM brain network

The nodes of the GM network were identified by using the Schaefer atlas with 400 regions [29], and the edges of the GM network were identified by using the KLS method. Finally, a 400 by 400 GM network was obtained for each individual subject. Please see the supplemental materials for details.

2.5. Topological analysis

This step was performed by using Gretna software version 2.0. Two network efficiency parameters [30], local efficiency (E_{loc}) and global efficiency (E_{glob}), and two nodal parameters, nodal degree [31] and nodal efficiency [32], were calculated to investigate the topological properties of individual GM networks. Please see the supplemental materials for details.

2.6. Gradient analysis

Gradient analysis was performed by using BrainSpace Toolbox [33]. Briefly, a group-level average connectivity matrix was first calculated based on the GM network of all subjects, and then ten group-level gradients were generated from the group-level average connectivity matrix. The parameters used for this step were set as follows, according to BrainSpace's documentation and previous studies [34,35]: dimension reduction technique = diffusion embedding, kernel = normalized angle, sparsity = 0.9. Furthermore, individual-level gradients were calculated by using the same parameters based on the individual GM network for each subject, and then the individual-level gradients were aligned to the group-level gradients by using Procrustes rotation to increase comparability across gradients. Similar to a previous study [36], we only focused on the principal gradient, which explained 26% of the variance, to maximize interpretability of this study. Finally, the principal gradient was plotted in the cortex for visualization. Please see Ref. [33] for additional details.

2.7. SVM model

The SVM model was constructed based on LIBSVM [37] and the Scikit-Learn library [38], with the GM network matrix of each subject as inputs. The participants were first split into ten separate, nonoverlapping subgroups, and the proportion of patients with MCI-C and MCI-NC was kept constant within each division. In each iteration, one subgroup was chosen as the test set, and the remaining patients were designated as the training set. Within each training set, a 10-fold stratified nested cross-validation was performed to obtain the optimal soft margin parameter C, which controls the trade-off between reducing training errors and having a large separation margin. The grid search method was used to find the best value for this parameter among $C = 10^{-3}$, 10^{-2}, 10^{-1}, 10°, 10^{1}, 10^{2}, 10^{3}, and 10^{4}. The parameter with the highest performance was chosen for training the SVM models. After the training of SVM models, the performance of the SVM model was assessed by using 10-fold stratified cross-validation with three measures: mean balanced accuracy, sensitivity and specificity. To obtain meaningful confidence intervals and P values, we examined the statistical significance of the model with a random permutation test (1000 times).

2.8. Statistical analysis

For the demographic, clinical and neuropsychological data, the group differences in sex and the number of APOE ε4 alleles were evaluated by using chi-square tests, while the group differences in other variables were all evaluated by using two-sample t tests with an alpha threshold of 0.05.

For network properties, ComBat [39] was first used to remove the inter-scanner variability, and then the gradient scores and topological properties between the MCI-C group and the MCI-NC group were compared by using two-sample t tests with a false discovery rate (FDR)-corrected alpha threshold of 0.05, with age as a covariate.

Partial correlations were calculated with age as a covariate to evaluate relationships between the gradient scores and nodal efficiency of brain regions with significant group diversity and the scores of neuropsychological tests as well as the number of APOE €4 alleles.

3. Results

3.1. Demographic and neuropsychological data and APOE ϵ4 alleles

Regarding the demographic data, the age of the MCI-C group was significantly higher than that of the MCI-NC group, while no significant differences in sex or years of education were found between the two groups. Regarding the proportion of individuals with APOE ϵ4 alleles, the MCI-C group had a much higher proportion of individuals with APOE 4 alleles than the MCI-NC group. Regarding the neuropsychological data, more serious cognitive impairment was detected in the MCI-C group for all of the neuropsychological tests than in the MCI-NC group. Detailed information is shown in Table 1.

3.2. Results of gradient analysis

The principal gradient showed a similar gradient axis from the DMN to the sensory-motor network (SMN) and visual network (VN) in both the MCI-C and MCI-NC groups (with similar variance explained in the two groups, two-sample *t*-test, $p = 0.704$) (Fig. 1a). However, distribution of the principal gradient scores in MCI-C group was significantly different from MCI-NC group (Kolmogorov−Smirnov test, $p = 0.031$). Global histograms (Fig. 1b) and box plots (Fig. 1c) were used to visually describe the differences in the distribution of gradient scores between the two groups. In the global histogram, fewer extreme values and more mid-range values were found in MCI-C group, compared with MCI-NC group, and in the box plots, both interquartile range (the difference between the upper quartile and the lower quartile) and range (the difference between the maximum and minimum values) in MCI-C group were less than MCI-NC group. Both global histograms and box plots suggested that distribution of the principal gradient in the MCI-C group was more compressed than that in the MCI-NC group. At the nodal level, three nodes (ROI_4, left lingual gyrus; ROI_201, right fusiform gyrus; ROI_205, right fusiform gyrus) in the VN and one node (ROI_152, left middle temporal gyrus) in the DMN showed increased gradient scores in the MCI-C group compared with the MCI-NC group ($p < 0.05$, FDR corrected) (Fig. 1d).

Moreover, the gradient scores of ROI_4 were significantly related with the MMSE ($r = -0.152$, $p = 0.017$) and ADAS-Cog13 ($r = 0.152$, $p = 0.017$) scores, the gradient scores of ROI_152 were significantly related with the RAVLT immediate recall ($r = -0.218$, $p = 0.001$), RAVLT percent forgetting ($r = 0.166$, $p = 0.009$), MoCA ($r = -0.216$, $p = 0.001$), ADAS-Cog13 ($r = 0.273$, $p < 0.001$) and ADAS-Cog11 ($r = 0.290$, $p < 0.001$) scores, as well as the number of APOE ϵ4 alleles ($r = 0.192$, $p = 0.002$), the gradient scores of ROI_201 were significantly related with the of MoCA ($r = -0.171$, $p = 0.007$), ADAS-Cog13 ($r = 0.176$, $p = 0.006$) and ADAS-Cog11 ($r = 0.178$, $p = 0.005$) scores, and the gradient scores of ROI_205 were significantly related with the of RAVLT immediate recall score ($r = -0.163$, $p = 0.010$) (Fig. 2).

3.3. Results of topological analysis

At the global level, no significant difference in E_{loc} or E_{glob} was detected between the two groups. At the nodal level, one node (ROI_40, left postcentral gyrus) in the SMN and two nodes (ROI_146, left anterior cingulate gyrus; ROI_358, right posterior cingulate gyrus) in the frontal parietal network (FPN) showed significantly decreased nodal efficiency, and one node (ROI_302, right temporal pole) in the ventral attention network (VAN) showed increased nodal efficiency in the MCI-C group compared with the MCI-NC group ($p < 0.05$, FDR corrected) (Fig. 3a). No significant difference in nodal degree was detected between the two groups.

Table 1
Demographic, neuropsychological and APOE ϵ4 alleles data.[a].

Variables	MCI-C	MCI-NC	P value[b]
Sample size	180	281	–
Age (years)[c]	73.82 ± 7.13	71.99 ± 7.33	0.008
Sex (M/F)	112/68	165/116	0.454
Education (years)	15.87 ± 2.81	16.06 ± 2.74	0.285
ADAS-Cog11	13.27 ± 4.68	8.78 ± 3.78	<0.001
ADAS-Cog13	21.38 ± 6.32	14.05 ± 5.76	<0.001
MMSE	26.78 ± 1.75	28.00 ± 1.69	<0.001
RAVLT immediate recall	27.29 ± 6.55	37.58 ± 9.87	<0.001
RAVLT learning	2.98 ± 2.27	4.64 ± 2.43	<0.001
RAVLT forgetting	5.02 ± 2.28	4.58 ± 2.49	<0.001
RAVLT percent forgetting	76.60 ± 28.09	53.11 ± 30.66	<0.001
MoCA	25.95 ± 2.70	26.35 ± 2.41	<0.001
Number of APOE ϵ4 alleles (0, 1, 2)	58, 92, 30	165, 93, 23	<0.001

Abbreviations: MCI-C = mild cognitive impairment patients who converted; MCI-NC = mild cognitive impairment patients who did not convert; ADAS-Cog = Alzheimer's Disease Assessment Scale-Cognitive subscale; MMSE = Mini Mental State Examination; RAVLT = Rey Auditory Verbal Learning Test; MoCA = Montreal Cognitive Assessment; APOE = apolipoprotein E.

[a] Data are presented as the mean ± standard deviation.

[b] P values for sex and number of APOE ϵ4 alleles were obtained by using chi-square tests, and p values for the other variables were obtained by using two-sample t-tests.

[c] Age was defined at the time of MRI scanning.

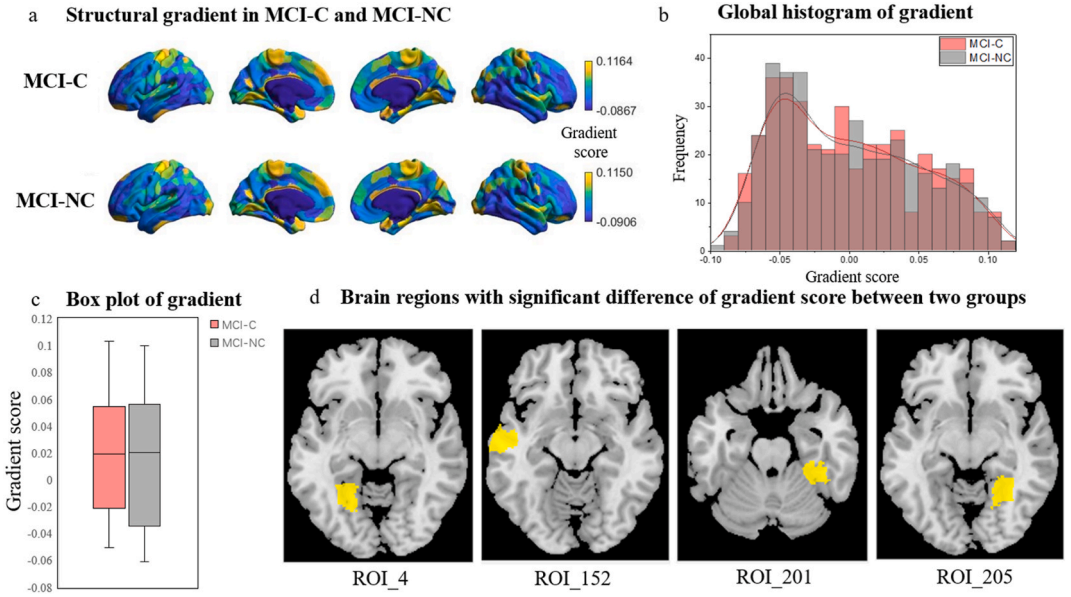

Fig. 1. (a) The principal gradient in the MCI-C and MCI-NC groups showed a similar gradient axis from the default mode network (blue) to the sensory-motor network and visual network (yellow). (b) The global histogram shows that the extreme values decreased and mid-range values increased in the MCI-C group compared with the MCI-NC group. (c) The boxplot had a smaller interquartile range and range for the MCI-C group than for the MCI-NC group (The upper boundary of the box represented the upper quartile of gradient scores, while the lower boundary represented the lower quartile, the line inside the box represented the median of the gradient scores, and the lengths of the whiskers represented the maximum and minimum values of the gradient scores). (d) The brain regions with significant differences (yellow) in gradient scores between the MCI-C and MCI-NC groups (ROI_4, left lingual gyrus; ROI_201, right fusiform gyrus; ROI_205, right fusiform gyrus; ROI_152, left middle temporal gyrus). (For interpretation of the references to colour in this figure legend, the reader is referred to the Web version of this article.)

Furthermore, the nodal efficiency of ROI_146 was significantly related to the RAVLT percent forgetting score ($r = -0.277$, $p = 0.027$). The nodal efficiency of ROI_358 was significantly related to the RAVLT percent forgetting score ($r = -0.252$, $p = 0.044$) (Fig. 3b).

3.4. *Performance of the SVM model*

In the classification of MCI-C and MCI-NC patients, we obtained a balanced accuracy of 79.4% ($p < 0.001$), and the sensitivity and specificity were 81.7% and 77.1%, respectively.

4. Discussion

In this study, we evaluated the differences in the GM network between the MCI-C and MCI-NC groups by combining gradient and topological analyses. In our gradient analysis, we found a similar principal gradient from the DMN to the SMN and VN in both the MCI-C and MCI-NC groups; this gradient was consistent with the principal gradient that was reported in a previous study [24]. However, the principal gradient in the MCI-C group was more compressed than that in the MCI-NC group, which suggested that the hierarchy of the GM network was more compressed in the MCI-C group. The hierarchy of the brain network was hypothesized to direct information flow throughout the brain, allowing sensory impulses to become progressively connected to other information and form more abstract representations [40], which is closely related to the general cognitive functioning [26]. Therefore, a more compressed hierarchy may be related to more serious cognitive impairment; this idea was consistent with the neuropsychological test scores measured in our study. At the nodal level, gradient scores of the left lingual gyrus, right fusiform gyrus and left middle temporal gyrus were increased in the MCI-C group, which were located at the two ends of the principal gradient. The lingual gyrus and fusiform gyrus both belong to the VN; the lingual gyrus is related to visual memory [41], and the fusiform gyrus is associated with face identification [42], both of which contribute to cognitive function [43,44]. The middle temporal gyrus belongs to the DMN and is associated with event representations [45], lexical comprehension [46] and semantic cognition [47]. These results further validated the relationship between the principal gradient and cognitive function.

In addition, the gradient scores of the left middle temporal gyrus were found to be related to both the number of APOE €4 alleles and neuropsychological test scores. The APOE €4 allele has been reported to be related to the formation of β-amyloid and neurofibrillary tangles [48,49], so more APOE ε4 alleles may cause more serious cerebral degeneration. It has been proven to be a risk factor for AD [50] and the most important predictor of longitudinal cognitive decline in elderly people [51]. Our study also suggested that the ratio of patients with APOE €4 alleles in the MCI-C group was much higher than that in the MCI-NC group. Thus, we can speculate that

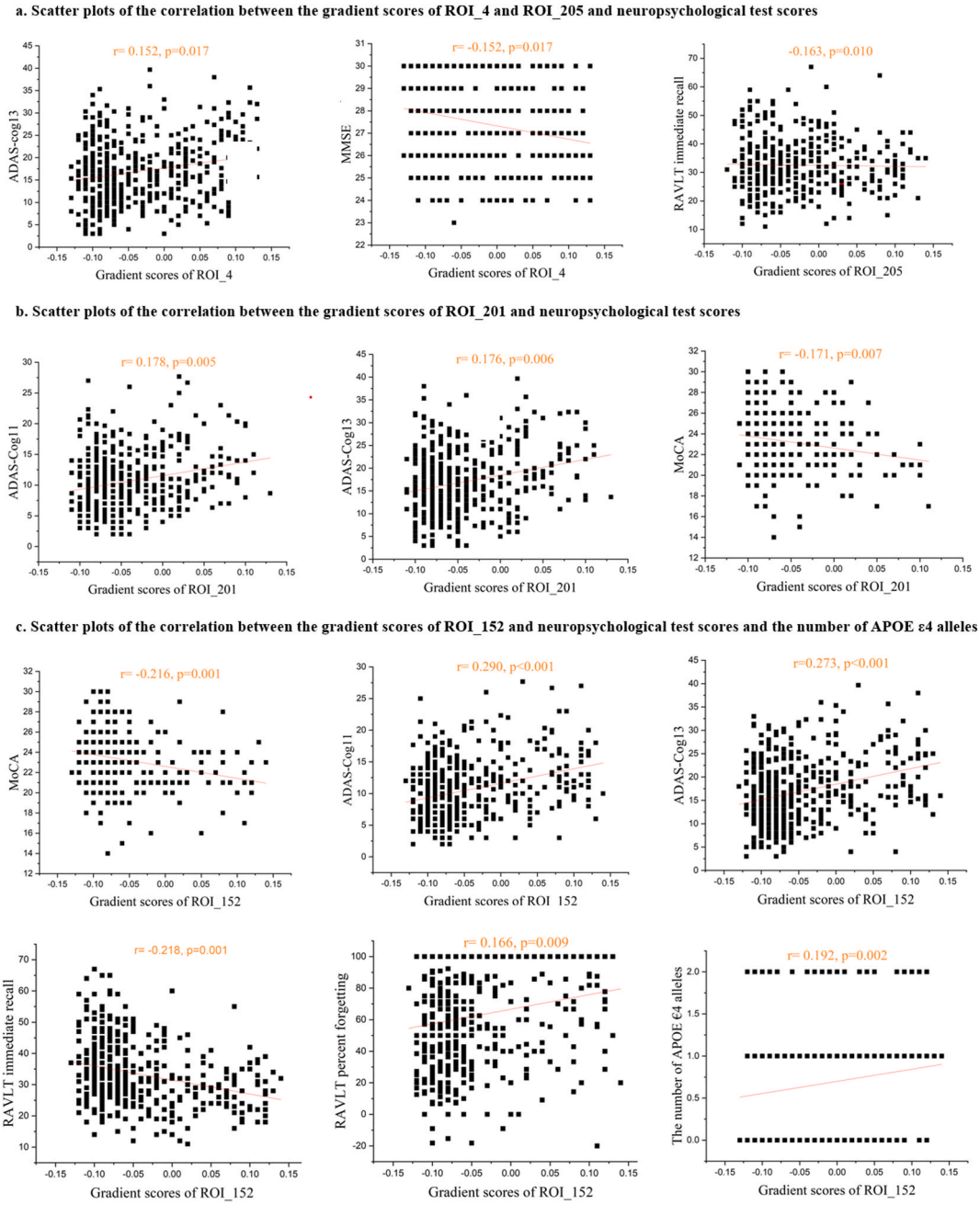

Fig. 2. Scatter plots of the correlation between the gradient scores and neuropsychological test scores and the number of APOE ε4 alleles. (a) Scatter plots of the correlation between the gradient scores of ROI_4 and ROI_205 and neuropsychological test scores. (b) Scatter plots of the correlation between the gradient scores of ROI_201 and neuropsychological test scores. (c) Scatter plots of the correlation between the gradient scores of ROI_152 and neuropsychological test scores and the number of APOE ε4 alleles. (ROI_4, left lingual gyrus; ROI_201, right fusiform gyrus; ROI_205, right fusiform gyrus; ROI_152, left middle temporal gyrus; MMSE, Mini-Mental State Examination; MoCA, Montreal Cognitive Assessment; RAVLT, Rey Auditory Verbal Learning Test; ADAS-Cog, Alzheimer's Disease Assessment Scale-Cognitive subscale; APOE, apolipoprotein E). Linear model fitting is shown over the scatterplot (red line). (For interpretation of the references to colour in this figure legend, the reader is referred to the Web version of this article.)

gradient scores of the left middle temporal gyrus may be a "bridge" to link APOE €4 alleles and cognitive impairment. Namely, more APOE €4 alleles cause more serious cerebral degeneration, which leads to alterations in gradient scores of the left middle temporal gyrus and then manifests as more serious cognitive impairment. Thus, gradient scores of the left middle temporal gyrus may be a potential biomarker to distinguish MCI-C and MCI-NC at baseline.

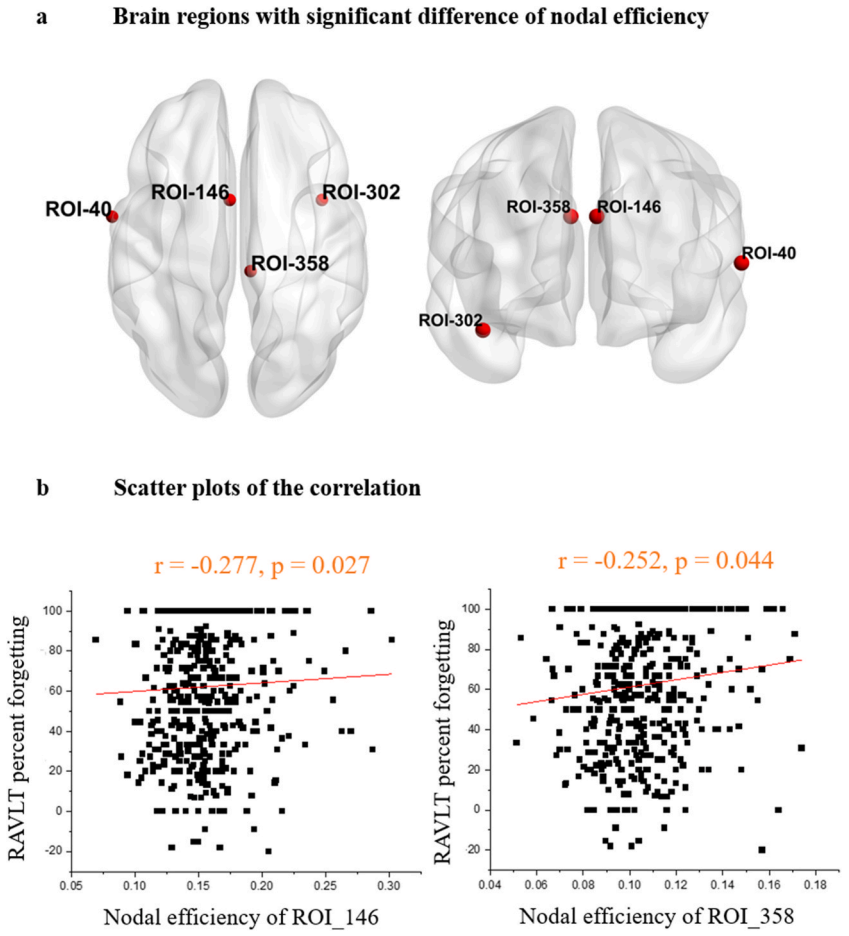

Fig. 3. (a) Brain regions with significant differences in nodal efficiency between the MCI-C and MCI-NC groups. (ROI_40, left postcentral gyrus; ROI_146, left anterior cingulate gyrus; ROI_358, right posterior cingulate gyrus; ROI_302, right temporal pole). (b) Scatter plots of the correlation between nodal efficiency and scores on neuropsychological tests. Linear model fitting is shown over the scatterplot (red line). (RAVLT, Rey Auditory Verbal Learning Test). (For interpretation of the references to colour in this figure legend, the reader is referred to the Web version of this article.)

In our topological analysis, compared with the MCI-NC group, the MCI-C group showed decreased nodal efficiency of nodes in the SMN and FPN and increased nodal efficiency of nodes in the VAN were detected in. Nodal efficiency characterizes the degree of information communication of adjacent nodes if a node is removed, which is also related to cognitive function [32]. Decreased nodal efficiency may be related to dysfunctions in information communication. Additionally, the SMN and FPN were located at the two ends of the principal gradient, so these results were consistent with our gradient analysis results. While the VAN is located in the middle area of the principal gradient, increased nodal efficiency of nodes in the VAN may be a compensatory effect. Furthermore, the nodal efficiency of the anterior cingulate gyrus and posterior cingulate gyrus were significantly related to the RAVLT percent forgetting scores. The RAVLT is a well-known measure of episodic memory [52], and the anterior cingulate gyrus and posterior cingulate gyrus have been reported to be related to the formation of episodic memory [53], consistent with our results.

In the classification of MCI-C and -MCI-NC by using an SVM model based on individual GM connectomes, we obtained a balanced accuracy of 79.4%, which is comparable to previous classification studies based on structural MRI. The results suggested that individual GM connectomes can be used as potential biomarkers to distinguish MCI-C and MCI-NC at baseline. However, the accuracy was still not satisfactory enough to meet the need for clinical diagnosis. Previous studies have reported that combining functional and structural MRI may improve the performance of the classification of MCI-C and MCI-NC [54,55], so we will try to combine the GM connectome and functional connectome to improve performance in the future.

Several limitations should be noted. First, to our knowledge, this is the first study to investigate the difference in the hierarchy of individual GM networks between the MCI-C and MCI-NC groups. Further studies are needed to investigate whether these differences can be replicated. Second, we observed differences in the principal gradient between the MCI-C and MCI-NC groups at baseline; however, it is still not clear whether these differences further develop with the progression of disease; therefore, a complete longitudinal follow-up study will be needed. Finally, we used the Schaefer atlas with 400 regions to construct the individual gray matter network; however, there is no widely accepted atlas for use in constructing brain networks, so other atlases should also be considered in future studies.

In conclusion, the hierarchy of the whole-brain GM network in the MCI-C group was more compressed than that in the MCI-NC group, which may be related to the more serious cognitive impairment in the MCI-C group. Furthermore, the gradient scores of the left middle temporal gyrus were both related to cognitive function and APOE ϵ4 alleles, thus making it a potential biomarker to distinguish MCI-C and MCI-NC at baseline.

Data availability statement

The data used in this study were downloaded from the Alzheimer's Disease Neuroimaging Initiative (ADNI) website (adni.loni.usc.edu), the data was collected in different institutions.The ADNI study was approved by an ethics committee on human experimentation at each institution, and written informed consent was obtained from all participants.

Ethics statement

Ethical review and approval were not required for the study on human participants because all the data in this study were downloaded from the Alzheimer's Disease Neuroimaging Initiative (ADNI) database.

CRediT authorship contribution statement

Baiwan Zhou: Writing – original draft, Visualization, Software, Methodology, Data curation. **Yueqi Zhao:** Formal analysis, Data curation. **Xiaojia Wu:** Writing – review & editing, Validation, Investigation.

Declaration of competing interest

The authors declare that they have no known competing financial interests or personal relationships that could have appeared to influence the work reported in this paper.

Acknowledgements

The authors would like to thank all the study participants and their families.

Appendix A. Supplementary data

Supplementary data to this article can be found online at https://doi.org/10.1016/j.heliyon.2024.e28874.

References

[1] C. Oboudiyat, H. Glazer, A. Seifan, C. Greer, R.S. Isaacson, Alzheimer's disease, Semin. Neurol. 33 (2013) 313–329, https://doi.org/10.1055/s-0033-1359319.
[2] M.S. Albert, S.T. DeKosky, D. Dickson, B. Dubois, H.H. Feldman, N.C. Fox, A. Gamst, D.M. Holtzman, W.J. Jagust, R.C. Petersen, P.J. Snyder, M.C. Carrillo, B. Thies, C.H. Phelps, The diagnosis of mild cognitive impairment due to Alzheimer's disease: recommendations from the national institute on aging-alzheimer's association workgroups on diagnostic guidelines for alzheimer's disease, Alzheimers Dement 7 (2011) 270–279, https://doi.org/10.1016/j.jalz.2011.03.008.
[3] R.C. Petersen, O. Lopez, M.J. Armstrong, T.S.D. Getchius, M. Ganguli, D. Gloss, G.S. Gronseth, D. Marson, T. Pringsheim, G.S. Day, M. Sager, J. Stevens, A. Rae-Grant, Practice guideline update summary: mild cognitive impairment: Report of the Guideline Development, Dissemination, and Implementation Subcommittee of the American Academy of Neurology, Neurology 90 (2018) 126–135, https://doi.org/10.1212/WNL.0000000000004826.
[4] H. Fukuda, H. Kanzaki, F. Murata, M. Maeda, M. Ikeda, Disease burden and progression in patients with New-onset mild cognitive impairment and alzheimer's disease identified from Japanese Claims data: Evidence from the LIFE study, J Alzheimers Dis 95 (2023) 1559–1572, https://doi.org/10.3233/JAD-230471.
[5] M.T. de Schotten, S.J. Forkel, The emergent properties of the connected brain, Science 378 (2022) 505–510, https://doi.org/10.1126/science.abq2591.
[6] O. Sporns, G. Tononi, R. Kötter, The human connectome: a structural description of the human brain, PLoS Comput. Biol. 1 (2005) e42, https://doi.org/10.1371/journal.pcbi.0010042.
[7] Y. He, Z.J. Chen, A.C. Evans, Small-world anatomical networks in the human brain revealed by cortical thickness from MRI, Cereb. Cortex 17 (2007) 2407–2419, https://doi.org/10.1093/cercor/bhl149.
[8] J. Seidlitz, F. Váša, M. Shinn, R. Romero-Garcia, K.J. Whitaker, P.E. Vértes, K. Wagstyl, P. Kirkpatrick Reardon, L. Clasen, S. Liu, A. Messinger, D.A. Leopold, P. Fonagy, R.J. Dolan, P.B. Jones, I.M. Goodyer, A. Raznahan, E.T. Bullmore, Morphometric similarity networks detect microscale cortical organization and predict inter-individual cognitive variation, Neuron 97 (1) (2018) 231–247.e7, https://doi.org/10.1016/j.neuron.2017.11.039.
[9] X. Lin, Y. Chen, M. Wang, C. Song, B. Lin, X. Yuan, Q. Liu, H. Yang, N. Jiang, Altered topological patterns of gray matter networks in Tinnitus: a graph-Theoretical-based study, Front. Neurosci. 14 (2020), https://doi.org/10.3389/fnins.2020.00541.
[10] H. Ding, Z. Wang, Y. Tang, T. Wang, M. Qi, W. Dou, L. Qian, Y. Gao, Q. Zhong, X. Yang, H. Tian, L. Zhang, Y. Zhu, Topological properties of individual gray matter morphological networks in identifying the preclinical stages of Alzheimer's disease: a preliminary study, Quant. Imag. Med. Surg. 13 (2023) 5258–5270, https://doi.org/10.21037/qims-22-1373.
[11] D.S. Bassett, E. Bullmore, B.A. Verchinski, V.S. Mattay, D.R. Weinberger, A. Meyer-Lindenberg, Hierarchical organization of human cortical networks in health and schizophrenia, J. Neurosci. 28 (2008) 9239–9248, https://doi.org/10.1523/jneurosci.1929-08.2008.
[12] A. Alexander-Bloch, J.N. Giedd, E. Bullmore, Imaging structural co-variance between human brain regions, Nat. Rev. Neurosci. 14 (2013) 322–336, https://doi.org/10.1038/nrn3465.
[13] B.M. Tijms, P. Seriès, D.J. Willshaw, S.M. Lawrie, Similarity-based extraction of individual networks from gray matter MRI scans, Cereb. Cortex 22 (2012) 1530–1541, https://doi.org/10.1093/cercor/bhr221.

[14] B.C. van Wijk, C.J. Stam, A. Daffertshofer, Comparing brain networks of different size and connectivity density using graph theory, PLoS One 5 (2010) e13701, https://doi.org/10.1371/journal.pone.0013701.

[15] X.Z. Kong, X. Wang, L. Huang, Y. Pu, Z. Yang, X. Dang, Z. Zhen, J. Liu, Measuring individual morphological relationship of cortical regions, J. Neurosci. Methods 237 (2014) 103–107, https://doi.org/10.1016/j.jneumeth.2014.09.003.

[16] X.Z. Kong, Z. Liu, L. Huang, X. Wang, Z. Yang, G. Zhou, Z. Zhen, J. Liu, Mapping individual brain networks using statistical similarity in regional Morphology from MRI, PLoS One 10 (2015) e0141840, https://doi.org/10.1371/journal.pone.0141840.

[17] H. Wang, X. Jin, Y. Zhang, J. Wang, Single-subject morphological brain networks: connectivity mapping, topological characterization and test-retest reliability, Brain Behav 6 (2016) e00448, https://doi.org/10.1002/brb3.448.

[18] X. Suo, D. Lei, N. Li, W. Li, G.J. Kemp, J.A. Sweeney, R. Peng, Q. Gong, Disrupted morphological grey matter networks in early-stage Parkinson's disease, Brain Struct. Funct. 226 (2021) 1389–1403, https://doi.org/10.1007/s00429-020-02200-9.

[19] X. Xu, P. Chen, Y. Xiang, Z. Xie, Q. Yu, X. Zhou, P. Wang, Altered pattern analysis and identification of subjective cognitive decline based on morphological brain network, Front. Aging Neurosci. 14 (2022) 965923, https://doi.org/10.3389/fnagi.2022.965923.

[20] D.J. Watts, S.H. Strogatz, Collective dynamics of 'small-world' networks, Nature 393 (1998) 440–442, https://doi.org/10.1038/30918.

[21] E. Dicks, W.M. van der Flier, P. Scheltens, F. Barkhof, B.M. Tijms, Single-subject gray matter networks predict future cortical atrophy in preclinical Alzheimer's disease, Neurobiol. Aging 94 (2020) 71–80, https://doi.org/10.1016/j.neurobiolaging.2020.05.008.

[22] E. Dicks, B.M. Tijms, M. ten Kate, A.A. Gouw, M.R. Benedictus, C.E. Teunissen, F. Barkhof, P. Scheltens, W.M. van der Flier, Gray matter network measures are associated with cognitive decline in mild cognitive impairment, Neurobiol. Aging 61 (2018) 198–206, https://doi.org/10.1016/j.neurobiolaging.2017.09.029.

[23] J.B. Pereira, M. Mijalkov, E. Kakaei, P. Mecocci, B. Vellas, M. Tsolaki, I. Kloszewska, H. Soininen, C. Spenger, S. Lovestone, A. Simmons, L.O. Wahlund, G. Volpe, E. Westman, Disrupted network topology in patients with stable and progressive mild cognitive impairment and alzheimer's disease, Cereb. Cortex 26 (2016) 3476–3493, https://doi.org/10.1093/cercor/bhw128.

[24] D.S. Margulies, S.S. Ghosh, A. Goulas, M. Falkiewicz, J.M. Huntenburg, G. Langs, G. Bezgin, S.B. Eickhoff, F.X. Castellanos, M. Petrides, E. Jefferies, J. Smallwood, Situating the default-mode network along a principal gradient of macroscale cortical organization, Proc. Natl. Acad. Sci. U. S. A. 113 (2016) 12574–12579, https://doi.org/10.1073/pnas.1608282113.

[25] J.M. Shine, M. Breakspear, P.T. Bell, K.A. Ehgoetz Martens, R. Shine, O. Koyejo, O. Sporns, R.A. Poldrack, Human cognition involves the dynamic integration of neural activity and neuromodulatory systems, Nat. Neurosci. 22 (2019) 289–296, https://doi.org/10.1038/s41593-018-0312-0.

[26] C. Murphy, H.-T. Wang, D. Konu, R. Lowndes, D.S. Margulies, E. Jefferies, J. Smallwood, Modes of operation: a topographic neural gradient supporting stimulus dependent and independent cognition, Neuroimage 186 (2019) 487–496, https://doi.org/10.1016/j.neuroimage.2018.11.009.

[27] S.J. Hong, R. Vos de Wael, R.A.I. Bethlehem, S. Lariviere, C. Paquola, S.L. Valk, M.P. Milham, A. Di Martino, D.S. Margulies, J. Smallwood, B.C. Bernhardt, Atypical functional connectome hierarchy in autism, Nat. Commun. 10 (2019) 1022, https://doi.org/10.1038/s41467-019-08944-1.

[28] A. Serrano-Pozo, S. Das, B.T. Hyman, APOE and Alzheimer's disease: advances in genetics, pathophysiology, and therapeutic approaches, Lancet Neurol. 20 (2021) 68–80, https://doi.org/10.1016/S1474-4422(20)30412-9.

[29] A. Schaefer, R. Kong, E.M. Gordon, T.O. Laumann, X.N. Zuo, A.J. Holmes, S.B. Eickhoff, B.T.T. Yeo, Local-global parcellation of the human cerebral cortex from intrinsic functional connectivity MRI, Cereb. Cortex 28 (2018) 3095–3114, https://doi.org/10.1093/cercor/bhx179.

[30] V. Latora, M. Marchiori, Efficient behavior of small-world networks, Phys. Rev. Lett. 87 (2001) 198701, https://doi.org/10.1103/PhysRevLett.87.198701.

[31] M. Rubinov, O. Sporns, Complex network measures of brain connectivity: uses and interpretations, Neuroimage 52 (2010) 1059–1069, https://doi.org/10.1016/j.neuroimage.2009.10.003.

[32] S. Achard, E. Bullmore, Efficiency and cost of economical brain functional networks, PLoS Comput. Biol. 3 (2007) e17, https://doi.org/10.1371/journal.pcbi.0030017.

[33] R.V. de Wael, O. Benkarim, C. Paquola, S. Lariviere, J. Royer, S. Tavakol, T. Xu, S.J. Hong, G. Langs, S. Valk, B. Misic, M. Milham, D. Margulies, J. Smallwood, B. C. Bernhardt, BrainSpace: a toolbox for the analysis of macroscale gradients in neuroimaging and connectomics datasets, Commun. Biol. 3 (2020) 103, https://doi.org/10.1038/s42003-020-0794-7.

[34] B. McKeown, W.H. Strawson, H.T. Wang, T. Karapanagiotidis, R. Vos de Wael, O. Benkarim, A. Turnbull, D. Margulies, E. Jefferies, C. McCall, B. Bernhardt, J. Smallwood, The relationship between individual variation in macroscale functional gradients and distinct aspects of ongoing thought, Neuroimage 220 (2020) 117072, https://doi.org/10.1016/j.neuroimage.2020.117072.

[35] A. Holmes, P.T. Levi, Y.C. Chen, S. Chopra, K.M. Aquino, J.C. Pang, A. Fornito, Disruptions of hierarchical cortical organization in early Psychosis and schizophrenia, Biol Psychiatry Cogn Neurosci Neuroimaging 8 (2023) 1240–1250, https://doi.org/10.1016/j.bpsc.2023.08.008.

[36] D. Dong, D. Yao, Y. Wang, S.J. Hong, S. Genon, F. Xin, K. Jung, H. He, X. Chang, M. Duan, B.C. Bernhardt, D.S. Margulies, J. Sepulcre, S.B. Eickhoff, C. Luo, Compressed sensorimotor-to-transmodal hierarchical organization in schizophrenia, Psychol. Med. 53 (2023) 771–784, https://doi.org/10.1017/s0033291721002129.

[37] C.-C. Chang, C.-J. Lin, LIBSVM: a library for support vector machines, ACM Trans. Intell. Syst. Technol. 2 (2011) 1–27, https://doi.org/10.1145/1961189.1961199.

[38] F. Pedregosa, G. Varoquaux, A. Gramfort, V. Michel, B. Thirion, O. Grisel, M. Blondel, P. Prettenhofer, R. Weiss, V. Dubourg, Scikit-learn: machine learning in python, J. Mach. Learn. Res. 12 (2011) 2825–2830.

[39] W.E. Johnson, C. Li, A. Rabinovic, Adjusting batch effects in microarray expression data using empirical Bayes methods, Biostatistics 8 (2007) 118–127, https://doi.org/10.1093/biostatistics/kxj037.

[40] P. Taylor, J.N. Hobbs, J. Burroni, H.T. Siegelmann, The global landscape of cognition: hierarchical aggregation as an organizational principle of human cortical networks and functions, Sci. Rep. 5 (2015) 18112, https://doi.org/10.1038/srep18112.

[41] J. Bogousslavsky, J. Miklossy, J.P. Deruaz, G. Assal, F. Regli, Lingual and fusiform gyri in visual processing: a clinico-pathologic study of superior altitudinal hemianopia, J. Neurol. Neurosurg. Psychiatry 50 (1987) 607–614, https://doi.org/10.1136/jnnp.50.5.607.

[42] L. Garrido, N. Furl, B. Draganski, N. Weiskopf, J. Stevens, G.C. Tan, J. Driver, R.J. Dolan, B. Duchaine, Voxel-based morphometry reveals reduced grey matter volume in the temporal cortex of developmental prosopagnosics, Brain 132 (2009) 3443–3455, https://doi.org/10.1093/brain/awp271.

[43] V. Cardin, E. Orfanidou, J. Rönnberg, C.M. Capek, M. Rudner, B. Woll, Dissociating cognitive and sensory neural plasticity in human superior temporal cortex, Nat. Commun. 4 (2013) 1473, https://doi.org/10.1038/ncomms2463.

[44] Y. Suzuki, C. Iseki, R. Igari, H. Sato, S. Koyama, H. Kawahara, H. Itagaki, Y. Sonoda, Y. Ohta, Reduced cerebral blood flow of lingual gyrus associated with both cognitive impairment and gait disturbance in patients with idiopathic normal pressure hydrocephalus, J. Neurol. Sci. 437 (2022) 120266, https://doi.org/10.1016/j.jns.2022.120266.

[45] A. Leshinskaya, S.L. Thompson-Schill, Transformation of event representations along middle temporal gyrus, Cereb. Cortex 30 (2020) 3148–3166, https://doi.org/10.1093/cercor/bhz300.

[46] J. Xu, J. Wang, L. Fan, H. Li, W. Zhang, Q. Hu, T. Jiang, Tractography-based parcellation of the human middle temporal gyrus, Sci. Rep. 5 (2015) 18883, https://doi.org/10.1038/srep18883.

[47] E.F. Chang, K.P. Raygor, M.S. Berger, Contemporary model of language organization: an overview for neurosurgeons, J. Neurosurg. 122 (2015) 250–261, https://doi.org/10.3171/2014.10.jns132647.

[48] D.E. Schmechel, A.M. Saunders, W.J. Strittmatter, B.J. Crain, C.M. Hulette, S.H. Joo, M.A. Pericak-Vance, D. Goldgaber, A.D. Roses, Increased amyloid beta-peptide deposition in cerebral cortex as a consequence of apolipoprotein E genotype in late-onset alzheimer disease, Proc. Natl. Acad. Sci. U. S. A. 90 (1993) 9649–9653, https://doi.org/10.1073/pnas.90.20.9649.

[49] T. Gomez-Isla, H.L. West, G.W. Rebeck, S.D. Harr, J.H. Growdon, J.J. Locascio, T.T. Perls, L.A. Lipsitz, B.T. Hyman, Clinical and pathological correlates of apolipoprotein E epsilon 4 in alzheimer's disease, Ann. Neurol. 39 (1996) 62–70, https://doi.org/10.1002/ana.410390110.

[50] C.C. Liu, C.C. Liu, T. Kanekiyo, H. Xu, G. Bu, Apolipoprotein E and alzheimer disease: risk, mechanisms and therapy, Nat. Rev. Neurol. 9 (2013) 106–118, https://doi.org/10.1038/nrneurol.2012.263.

[51] J. Corley, F. Conte, S.E. Harris, A.M. Taylor, P. Redmond, T.C. Russ, I.J. Deary, S.R. Cox, Predictors of longitudinal cognitive ageing from age 70 to 82 including APOE e4 status, early-life and lifestyle factors: the lothian birth cohort 1936, Mol. Psychiatry 28 (2023) 1256–1271, https://doi.org/10.1038/s41380-022-01900-4.

[52] A. Estévez-González, J. Kulisevsky, A. Boltes, P. Otermín, C. García-Sánchez, Rey verbal learning test is a useful tool for differential diagnosis in the preclinical phase of alzheimer's disease: comparison with mild cognitive impairment and normal aging, Int. J. Geriatr. Psychiatry 18 (2003) 1021–1028, https://doi.org/10.1002/gps.1010.

[53] E.T. Rolls, The cingulate cortex and limbic systems for emotion, action, and memory, Brain Struct. Funct. 224 (2019) 3001–3018, https://doi.org/10.1007/s00429-019-01945-2.

[54] H.I. Suk, S.W. Lee, D. Shen, Latent feature representation with stacked auto-encoder for AD/MCI diagnosis, Brain Struct. Funct. 220 (2015) 841–859, https://doi.org/10.1007/s00429-013-0687-3.

[55] S.H. Hojjati, A. Ebrahimzadeh, A. Babajani-Feremi, Identification of the early stage of alzheimer's disease using structural MRI and resting-state fMRI, Front. Neurol. 10 (2019) 904, https://doi.org/10.3389/fneur.2019.00904.